JOURNAL OF Materials CHEMISTRY

Crystal structures and magnetic properties of ordered perovskites Ba_2LnIrO_6 (Ln = lanthanide)

Makoto Wakeshima,* Daijitsu Harada and Yukio Hinatsu

Division of Chemistry, Graduate School of Science, Hokkaido University, Sapporo 060-0810, Japan. E-mail: wake@sci.hokudai.ac.jp

Received 20th September 1999, Accepted 1st December 1999

The crystal structures and magnetic properties of ordered perovskites Ba_2LnIrO_6 (Ln = lanthanide) are reported. They were determined to have monoclinic perovskite-type structures with space group $P2_1/n$. Their magnetic susceptibilities were measured from 2 to 350 K. Ba_2CeIrO_6 and Ba_2PrIrO_6 show antiferromagnetic transitions at 17 and 71 K, respectively. In these compounds, the Ce and Pr ions are found to be in the tetravalent state from analysis of their crystal structures and magnetic susceptibilities.

Introduction

Perovskites or perovskite-like oxides containing platinum metals often exhibit interesting magnetic and electrical properties. Strontium ruthenates, $Sr_{n+1}Ru_nO_{3n+1}$, show interesting behavior, for example $SrRuO_3$ transforms to the ferromagnetic state below 160 K[1] and Sr_2RuO_4 is a superconductor below 1 K.[2] Many compounds containing iridium show magnetic ordering, for example Sr_2IrO_4 and $BaIrO_{3-\delta}$ show a weak ferromagnetic transition at 250 K[3] and a ferromagnetic transition at 180 K,[4] respectively.

We have been studying the structural chemistry and magnetic properties of ordered perovskites containing both lanthanides and ruthenium (iridium), $A_2LnB'O_6$ (A = Sr, Ba; Ln = lanthanide; B′ = Ru, Ir). These compounds show structural ordering between B site cations, lanthanide elements and Ru(Ir). Recently, Doi and Hinatsu reported the crystal structures and magnetic properties of a series of Sr_2LnRuO_6 compounds, which showed unique magnetic behavior at low temperatures.[5] In these compounds, lanthanide and ruthenium ions are in the trivalent and pentavalent states, respectively. Previously, we reported the preparation, crystal structures, and magnetic properties of iridium perovskites Sr_2LnIrO_6.[6] Through their X-ray diffraction measurements, we have found that although the lattice parameters for Sr_2LnIrO_6 increase smoothly with the ionic radius of Ln^{3+}, those for Sr_2CeIrO_6 and Sr_2TbIrO_6 deviate significantly from this trend. To rationalize these experimental results, we have suggested that the Ce and Tb ions are not in the trivalent state, but are rather tetravalent and that the Ir ions are also tetravalent. Sr_2CeIrO_6 and Sr_2TbIrO_6 show antiferromagnetic transitions at 21 and 51 K, respectively.

In this study, we prepared a series of Ba_2LnIrO_6 compounds and determined their crystal structures. Through magnetic susceptibility measurements, Ba_2CeIrO_6 and Ba_2PrIrO_6 were found to undergo antiferromagnetic transitions at low temperatures.

Experimental

A series of Ba_2LnIrO_6 compounds (Ln = La–Nd, Sm–Lu) was synthesized by a solid state reaction process. Powders of barium carbonate ($BaCO_3$), iridium metal (Ir) and lanthanide sesquioxide Ln_2O_3 (except for Ln = Ce, Pr and Tb) each with a purity of > 99.9% were used as starting materials. In the case of Ln = Ce, Pr, and Tb, CeO_2, Pr_6O_{11} and Tb_4O_7 were used. In order to remove any moisture, La_2O_3 and Nd_2O_3 were preheated in air at 1073 K. The stoichiometric mixtures were ground, pelletized and calcined at a temperature of 1173 K. The calcined materials were reground and sintered in air at 1473 K for several days with several intervening regrinding and repelletizing steps.

X-Ray diffraction measurements were carried out at room temperature in the range $10 \leqslant 2\theta/^\circ \leqslant 120$ using a 2θ step size of 0.02° with graphite-monochromated Cu-Kα radiation on a Rigaku RINT2200 diffractometer. Rietveld analyses were carried out with the program RIETAN-97[7] using collected diffraction data.

The temperature dependence of the magnetic susceptibilities was measured under both zero-field-cooled condition (ZFC) and field-cooled condition (FC) in the temperature range 2–350 K using a SQUID magnetometer (Quantum Design, MPMS-5S). The ZFC susceptibility measurements were performed under an applied magnetic field of 0.1 T, after the sample was cooled from 300 to 2 K in zero field. For FC susceptibility measurements, the sample was cooled in the presence of a field of 0.1 T. For the Ba_2CeIrO_6 and Ba_2PrIrO_6 compounds, detailed temperature dependence of the susceptibilities was measured in the neighborhood of the magnetic transition temperatures. The magnetization was measured at 2 K by changing the applied magnetic field between −5 and 5 T.

For the Ba_2CeIrO_6 and Ba_2PrIrO_6 compounds, heat capacity measurements were carried out using a relaxation technique supplied by the commercial heat capacity measurement system (Quantum Design, PPMS) in the temperature range 2–120 K. The sample in the form of pellet (*ca.* 10 mg) was mounted on an alumina plate with Apiezon for better thermal contact.

Results and discussion

Crystal structures

The results of the X-ray diffraction measurements show that Ba_2LnIrO_6 compounds were found to form in a single phase for all the lanthanides. Rietveld analysis was performed with the program RIETAN to obtain powder X-ray diffraction profiles. All XRD patterns of Ba_2LnIrO_6 could be fitted with perovskite-type monoclinic structures (space group $P2_1/n$) with positionally ordered arrangements between the B site ions, Ln and Ir ions. The relation between the lattice constants of this unit cell and that of the primitive perovskite unit cell (a_p) with cubic structure are given by $a \approx \sqrt{2}a_p$, $b \approx \sqrt{2}a_p$ and $c \approx 2a_p$.

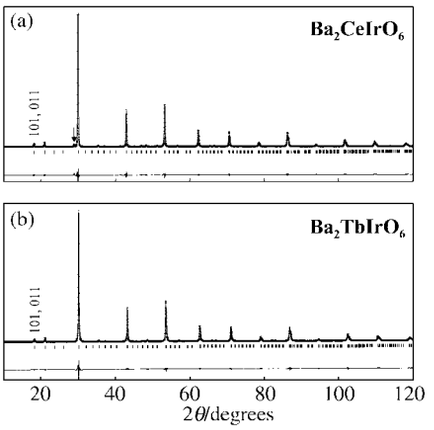

Fig. 1 X-Ray diffraction profiles for Ba_2CeIrO_6 (a) and Ba_2TbIrO_6 (b). The calculated and observed diffraction profiles are shown on the top solid line and cross markers, respectively. The vertical marks in the middle show positions calculated for Bragg reflections. The bottom trace is a plot of the difference between calculated and observed intensities. An arrow in the profile of Ba_2CeIrO_6 corresponds to a diffraction peak for CeO_2 impurity.

According to the Rietveld refinement, the Ln and Ir ions were found to fully occupy the 2*c* (0, 1/2, 0) and 2*d* (1/2, 0, 0) sites, respectively. Fig. 1 shows the results of XRD pattern fitting for Ba_2CeIrO_6 and Ba_2TbIrO_6. The presence of the (011) reflection at 2θ *ca.* 19° shows the ordered arrangements between the B site ions. A small amount of CeO_2 was present in the Ba_2CeIrO_6 sample as shown in Fig. 1(a). Since CeO_2 is diamagnetic, its effect on the magnetic susceptibility is negligibly small. The crystal structure of Ba_2CeIrO_6 after refinement is illustrated in Fig. 2. Both iridium and cerium ions are octahedrally coordinated by six oxygen ions with their octahedra being arranged in an alternate manner. Table 1 lists the lattice parameters of the series of Ba_2LnIrO_6 compounds. The variation of lattice parameters and cell volumes with the ionic radius of Ln^{3+} is shown in Fig. 3 and are found to increase monotonously with the ionic radius of the Ln^{3+} ion from Lu to La. However, the lattice parameters for Ba_2CeIrO_6 and Ba_2PrIrO_6 deviate substantially from this trend. Fig. 4 shows the variation of the average Ir–O and Ln–O bond lengths for the Ba_2LnIrO_6 compounds *vs.* the ionic radius of Ln^{3+}. Except for Ba_2CeIrO_6 and Ba_2PrIrO_6, it is found that the average Ln–O length increases with the ionic radius of Ln^{3+} while the average Ir–O bond length is nearly constant (*ca.* 1.98 Å). However, those for Ba_2CeIrO_6 and Ba_2PrIrO_6 deviate

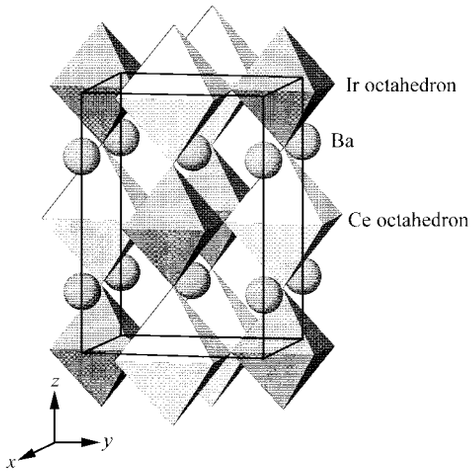

Fig. 2 The structure of Ba_2CeIrO_6. Spheres are Ba atoms, bright octahedra are CeO_6 units and dark octahedra are IrO_6 units.

from this trend. The refined Ce–O and Pr–O bond lengths are 2.193 and 2.175 Å, respectively. According to Shannon's ionic radii,[8] Ce^{4+}–O^{2-}, Ce^{3+}–O^{2-}, Pr^{3+}–O^{2-} and Pr^{4+}–O^{2-} bond lengths are calculated to be 2.27, 2.41, 2.25 and 2.39 Å, respectively. The observed Ln–O bond lengths for Ba_2LnIrO_6 (Ln = Ce and Pr) are close to Ln^{4+}–O^{2-} lengths rather than Ln^{3+}–O^{2-} lengths. In addition, the Ir–O lengths for Ba_2CeIrO_6 and Ba_2PrIrO_6 are longer than expected for Ir^{5+}–O^{2-} (1.97 Å) and are closer to the value for Ir^{4+}–O^{2-} (2.025 Å). These results indicate that the Ce and Pr ions in Ba_2LnIrO_6 (Ln = Ce and Pr) are tetravalent with the Ir ions also tetravalent.

In this study, it is found that for Ba_2TbIrO_6, the oxidation state of terbium is trivalent and that of iridium is pentavalent. On the other hand, our previous study on Sr_2TbIrO_6 shows that both the terbium and iridium ions are tetravalent.[6] The question arises as to why this discrepancy occurs *i.e.* as to why some compounds exist as $A_2Ln^{4+}Ir^{4+}O_6$ rather than $A_2Ln^{3+}Ir^{5+}O_6$. The stability of perovskites is generally estimated by the tolerance factor *t*. For an ordered perovskite compound, $A_2B'B''O_6$, this factor is defined by eqn. (1)

$$t = \frac{r_A + r_O}{\sqrt{2}\left(\frac{r_{B'} + r_{B''}}{2}\right) + r_O} \quad (1)$$

where r_A, $r_{B'}$, $r_{B''}$ and r_O are the radii of the A, B′ and B″ metal ions and oxygen ion, respectively. For an ideal cubic perovskite structure, the value of *t* is equal to unity, whereas for structures distorted from cubic symmetry, the value of *t* is <1. Usually, the perovskite phase is stable for *t* in the range of *ca.* 0.8–1. Tolerance factors *t* for A_2LnIrO_6 (A = Sr and Ba; Ln = Ce, Pr and Tb) are listed in Table 2. The tolerance value for $Ba_2Tb^{4+}Ir^{4+}O_6$ is >1 which destabilizes this phase relative to the $Ba_2Tb^{3+}Ir^{5+}O_6$ perovskite phase. Table 2 lists tolerance factors for both $A_2Ln^{3+}Ir^{5+}O_6$ and $A_2Ln^{4+}Ir^{4+}O_6$ phases. The values for $BaLn^{4+}Ir^{4+}O_6$ (Ln = Ce or Pr) are nearer to unity than those for $Ba_2Ln^{3+}Ir^{5+}O_6$, which suggests that the ionic model $Ba_2Ln^{4+}Ir^{4+}O_6$ (Ln = Ce or Pr) is more stable. This result is consistent with the experimental lattice parameters of these compounds and the Ln–O (Ln = Ce or Pr) and Ir–O bond lengths.

Magnetic susceptibilities

The results of magnetic susceptibility measurements for Ba_2LnIrO_6 (except Ln = Ce or Pr) show paramagnetic behavior down to 2 K. We have already published the magnetic properties of Ba_2LaIrO_6 and Ba_2LuIrO_6 in which only the iridium ions are magnetic, and their magnetic behavior was found to follow Kotani's theory.[9] The magnetic properties of Ba_2LnIrO_6 (Ln = Sm, Eu, Gd and Yb) were also reported elsewhere.[10] Table 3 summarizes the results of magnetic susceptibility measurements. The temperature dependence of the reciprocal magnetic susceptibility of Ba_2TbIrO_6 is shown in Fig. 5 and no evidence of any magnetic transition was observed down to 2 K. The effective magnetic moment of Ba_2TbIrO_6 is calculated to be $9.71\mu_B$ from the reciprocal susceptibility *vs.* temperature curve in good agreement with the theoretical moment for free Tb^{3+} ($\mu_{eff} = 9.72\mu_B$). In Ba_2TbIrO_6, both Tb^{3+} and Ir^{5+} ions are magnetic and thus should both contribute to the magnetic properties. However, the magnetic contribution of the Ir^{5+} ion to the paramagnetic behavior should be quite small.

The magnetic moment of the Ir^{5+} ion is estimated from the magnetic susceptibility data of Ba_2LaIrO_6 and Ba_2LuIrO_6 in which only the Ir^{5+} ions are magnetic.[9] The magnetic moment of the Ir^{5+} ion changes with temperature being $0.2\mu_B$ at 2 K and $1.5\mu_B$ at 320 K. Since the magnetic susceptibility is proportional to the square of the effective magnetic moments, and since the moment of the Ir^{5+} ion is much smaller than that of the free Tb^{3+} ion, the contribution of the Ir^{5+} ion to the

Table 1 Lattice parameters, cell volumes and R factors for Ba_2LnIrO_6

	a/Å	b/Å	c/Å	β/°	V/Å^3	R_{wp}[a] (%)	R_I[b] (%)
Ba_2LaIrO_6	6.0510(3)	6.0603(3)	8.5737(4)	90.297(3)	314.32(2)	9.43	1.12
Ba_2CeIrO_6	5.9663(4)	5.9567(3)	8.4266(7)	89.986(7)	299.47(4)	10.47	2.64
Ba_2PrIrO_6	5.9443(3)	5.9379(2)	8.3984(8)	89.979(8)	296.44(2)	12.51	1.52
Ba_2NdIrO_6	6.0008(2)	5.9999(2)	8.4843(3)	90.042(2)	305.75(2)	13.28	2.67
Ba_2SmIrO_6	5.9731(9)	5.9718(8)	8.4468(6)	90.030(8)	301.03(6)	13.67	1.88
Ba_2EuIrO_6	5.9615(7)	5.9588(6)	8.4231(6)	90.001(5)	299.31(6)	13.16	1.90
Ba_2GdIrO_6	5.9504(6)	5.9467(6)	8.4108(7)	90.005(4)	297.80(5)	13.06	1.88
Ba_2TbIrO_6	5.9319(3)	5.9227(3)	8.3866(5)	90.01(1)	294.65(3)	13.67	1.96
Ba_2DyIrO_6	5.9245(3)	5.9186(3)	8.3653(4)	90.01(1)	293.33(3)	12.25	1.84
Ba_2HoIrO_6	5.9139(2)	5.9048(2)	8.3501(3)	89.981(8)	291.59(2)	9.43	1.29
Ba_2ErIrO_6	5.8988(5)	5.8899(4)	8.3319(8)	89.982(9)	289.81(4)	11.95	2.52
Ba_2TmIrO_6	5.8916(2)	5.8799(2)	8.3148(2)	89.974(9)	288.04(2)	12.37	1.82
Ba_2YbIrO_6	5.8793(2)	5.8682(2)	8.3010(3)	89.969(9)	286.40(2)	11.41	1.98
Ba_2LuIrO_6	5.8689(2)	5.8608(2)	8.2885(3)	89.994(6)	285.13(2)	12.11	1.37

[a] $R_{wp}=[\Sigma w(|F_o|-|F_c|)^2/\Sigma w|F_o|^2]^{1/2}$. [b] $R_I=\Sigma|I_{ko}-I_{kc}|/\Sigma I_{ko}$.

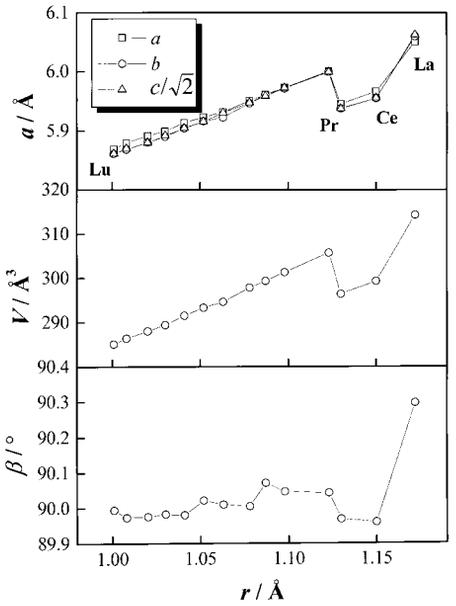

Fig. 3 Variation of lattice parameters and cell volumes for Ba_2LnIrO_6 with the ionic radius of Ln^{3+}.

paramagnetic susceptibility of Ba_2TbIrO_6 is negligibly small (at most 2.3% even at 320 K), *i.e.* paramagnetic behavior of Ba_2TbIrO_6 is essentially attributable to the moment of Tb^{3+} ion.

Fig. 6 shows the temperature dependence of the reciprocal magnetic susceptibility for Ba_2CeIrO_6. The susceptibility curve indicates antiferromagnetic behavior below 17 K and yields an effective magnetic moment $\mu_{eff}=1.30\mu_B$ with a Weiss constant $\theta=-177$ K above 30 K. The absence of divergence between the

Table 2 Tolerance factors t for A_2LnIrO_6

	$t(A_2Ln^{3+}Ir^{5+}O_6)$	$t(A_2Ln^{4+}Ir^{4+}O_6)$
Sr_2CeIrO_6	0.917	0.935
Ba_2CeIrO_6	0.972	0.991
Ba_2PrIrO_6	0.976	0.996
Sr_2TbIrO_6	0.935	0.959
Ba_2TbIrO_6	0.992	1.017

Table 3 Magnetic properties of Ba_2LnIrO_6[a]

		T_N/K	μ_{eff}(exptl.)/μ_B	μ_{eff}(theor.)/μ_B
Ba_2CeIrO_6	AF	17	(1.30)[b]	(1.73)[b]
Ba_2PrIrO_6	AF	71	2.21 (1.30)[b]	2.54 (1.73)[b]
Ba_2NdIrO_6	P		3.67	3.62
Ba_2SmIrO_6	P		—	—
Ba_2EuIrO_6	P		—	—
Ba_2GdIrO_6	P		7.63	7.94
Ba_2TbIrO_6	P		9.71	9.72
Ba_2DyIrO_6	P		9.90	10.65
Ba_2HoIrO_6	P		9.99	10.62
Ba_2ErIrO_6	P		9.08	9.58
Ba_2TmIrO_6	P		7.34	7.56
Ba_2YbIrO_6	P		4.54	4.54

[a] AF: Antiferromagnetism; P: paramagnetism. [b] For Ba_2CeIrO_6 and Ba_2PrIrO_6, values in parentheses are the effective magnetic moments of the Ir^{4+} ion.

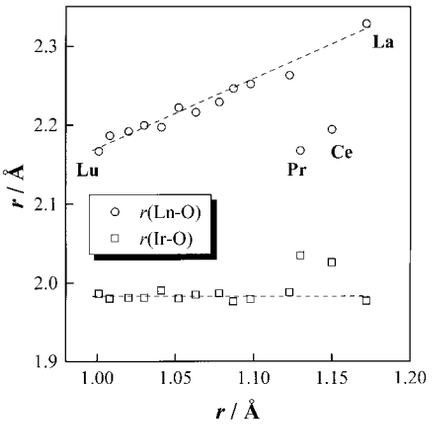

Fig. 4 Variation of average bond lengths Ln–O and Ir–O for Ba_2LnIrO_6 with the ionic radius of Ln^{3+}.

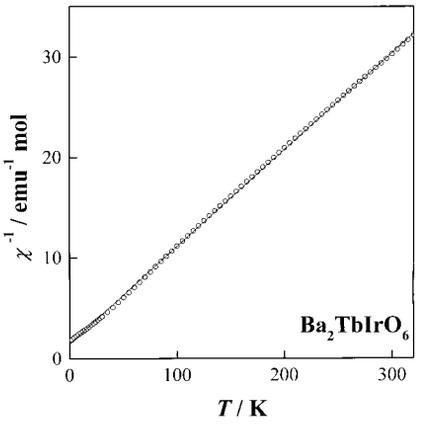

Fig. 5 Temperature dependence of the reciprocal magnetic susceptibility of Ba_2TbIrO_6.

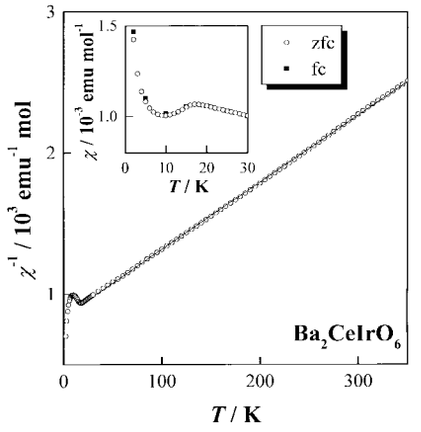

Fig. 6 Temperature dependence of the reciprocal magnetic susceptibility of Ba_2CeIrO_6. Inset shows the temperature dependence of the magnetic susceptibility.

ZFC and FC magnetic susceptibilities or of magnetic hysteresis in the magnetization *vs.* magnetic field curve indicate that below 17 K this compound transforms to an antiferromagnetic state without weak ferromagnetic properties. For Ba_2CeIrO_6, the cerium ion is tetravalent state, *i.e.* is diamagnetic, and the tetravalent iridium ion is the only paramagnetic ion. The $5d^5$ electrons of the Ir^{4+} ions in Ba_2CeIrO_6 are expected to be localized rather than itinerant. The Ir^{4+} ion in low spin configuration has a $t_{2g}^5e_g^0$ electron configuration (the total spin quantum number is $S=1/2$) and its effective magnetic moment, μ_{eff}, is calculated to be $1.73\mu_B$ from the spin-only formula. The moment obtained experimentally ($1.30\mu_B$) is smaller than this value owing to crystal field effects and/or covalency in the Ir–O bonds.

Fig. 7 shows the magnetic susceptibility of Ba_2PrIrO_6 as a function of temperature. This compound shows antiferromagnetic behavior below 71 K and no divergence between the ZFC and FC susceptibilities. The Néel temperature of this compound is much higher than that of Ba_2CeIrO_6. For Ba_2CeIrO_6, the nearest-neighbor magnetic interaction is the superexchange interaction along the pathway Ir–O–O–Ir. For Ba_2PrIrO_6, the magnetic interaction pathway should be *via* Ir–O–Pr–O–Ir, with the $4f^1$ electron of the Pr^{4+} ion enhancing the interactions greatly. If we assume the effective magnetic

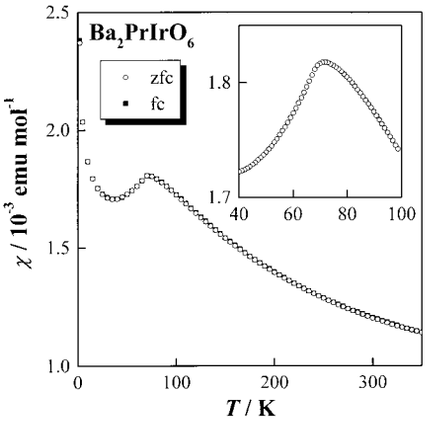

Fig. 7 Temperature dependence of the magnetic susceptibility of Ba_2PrIrO_6.

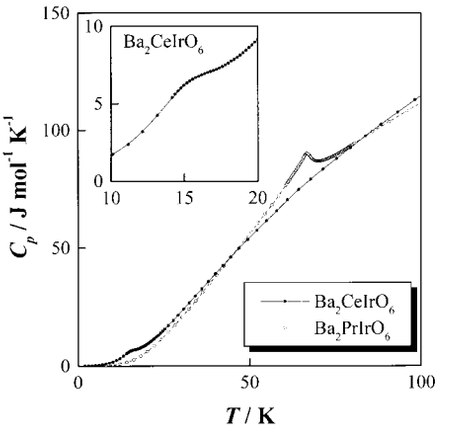

Fig. 8 Temperature dependence of the heat capacity of Ba_2CeIrO_6 and Ba_2PrIrO_6.

moment of the Ir^{4+} ion in Ba_2PrIrO_6 is $1.30\mu_B$, the value obtained from the susceptibility of Ba_2CeIrO_6, the moment of the Pr^{4+} ion is calculated to be $2.21\mu_B$ above 100 K from the equation $\chi=N_A[\mu_{eff}(Ir^{4+})^2+\mu_{eff}(Pr^{4+})^2]/3k_BT$. This value is smaller than the theoretical moment for the free Pr^{4+} ion ($2.54\mu_B$) with Pr^{4+} ions also affected by crystal field effects.

Heat capacity

Fig. 8 shows the variation of the heat capacity for Ba_2LnIrO_6 (Ln = Ce or Pr) as a function of temperature. Both compounds show a heat capacity anomaly at low temperatures. Ba_2CeIrO_6 shows a very broad maximum at *ca.* 16 K, corresponding to the maximum of magnetic susceptibility *vs.* temperature curve at 17 K (Fig. 6). The heat capacity of Ba_2PrIrO_6 has a λ-type anomaly at 67 K, indicating the existence of a second order phase transition. This is in accord with the behavior found for the magnetic susceptibility, *i.e.*, this compound shows a maximum in the susceptibility *vs.* temperature curve at 71 K, as shown in Fig. 7. From the magnetic susceptibility and heat capacity measurements, it is confirmed that Ba_2CeIrO_6 and Ba_2PrIrO_6 transform into antiferromagnetic states at low temperatures.

References

1 A. Callaghan, C. W. Moeller and R. Ward, *Inorg. Chem.*, 1966, **5**, 1572.
2 Y. Maeno, H. Hashimoto, K. Yoshida, S. Nishizaki, T. Fujita, J. G. Bednorz and F. Lichtenberg, *Nature*, 1994, **372**, 532.
3 M. K. Crawford, M. A. Subramanian, R. L. Harlow, J. A. Fernandez-Baca, Z. R. Wang and D. C. Johnston, *Phys. Rev. B*, 1994, **49**, 9198.
4 A. V. Powell and P. D. Battle, *J. Alloys Compd.*, 1993, **191**, 313.
5 Y. Doi and Y. Hinatsu, *J. Phys.: Condens. Matter.*, 1999, **11**, 4813.
6 D. Harada, M. Wakeshima and Y. Hinatsu, *J. Solid State Chem.*, 1999, **145**, 356.
7 F. Izumi, in *The Rietveld Method*, ed. R. A. Young, Oxford University Press, Oxford, 1993, ch. 13.
8 R. D. Shannon, *Acta Crystallogr., Sect. A*, 1976, **32**, 751.
9 M. Wakeshima, D. Harada and Y. Hinatsu, *J. Alloys Compd.*, 1999, **287**, 130.
10 M. Wakeshima, D. Harada Y. Hinatsu and N. Masaki, *J. Solid State Chem.*, 1999, **147**, 618.

Paper a907586k